Bioelectrochemistry 143 (2022) 107987

Contents lists available at ScienceDirect

Bioelectrochemistry

journal homepage: www.elsevier.com/locate/bioelechem

Electric-driven membrane poration: A rationale for water role in the kinetics of pore formation

Paolo Marracino [a], Laura Caramazza [b,c,1], Maria Montagna [b,d,1], Ramin Ghahri [b], Marco D'Abramo [d], Micaela Liberti [b,c], Francesca Apollonio [b,c,*]

[a] Rise Technology S.r.l., L.re Paolo Toscanelli 170, 00121 Rome, Italy
[b] Department of Information Engineering, Electronics and Telecommunications, Sapienza University of Rome, Rome, Italy
[c] Center for Life Nano- & Neuro-Science, Fondazione Istituto Italiano di Tecnologia (IIT), 00161 Rome, Italy
[d] Department of Chemistry, Sapienza Sapienza University of Rome, Rome, Italy

ARTICLE INFO

Article history:
Received 1 December 2020
Received in revised form 19 October 2021
Accepted 20 October 2021
Available online 26 October 2021

Keywords:
Biological Phenomena
Electroporation
Pore
Kinetics
Lipid Bilayers
Molecular Dynamics Simulation

ABSTRACT

Electroporation is a well-established technique used to stimulate cells, enhancing membrane permeability by inducing reversible membrane pores. In the absence of experimental observation of the dynamics of pore creation, molecular dynamics studies provide the molecular-level evidence that the electric field promotes pore formation. Although single steps in the pore formation process are well assessed, a kinetic model representing the mathematical description of the electroporation process, is lacking.

In the present work we studied the basis of the pore formation process, providing a rationale for the definition of a first-order kinetic scheme. Here, authors propose a three-state kinetic model for the process based on the assessed mechanism of water defects intruding at the water/lipid interface, when applying electric field intensities at the edge of the linear regime. The methodology proposed is based on the use of two robust biophysical quantities analyzed for the water molecules intruding at the water/lipid interface: (i) number of hydrogen bonds; (ii) number of contacts. The final model, sustained by a robust statistical sampling, provides kinetic constants for the transitions from the intact bilayer state to the hydrophobic pore state.

1. Introduction

Cells and organelles are protected by thin membranes, composed of a double lipid layer with embedded and adsorbed membrane proteins, that separate their chemical contents from the extracellular environment. These membranes act as a barrier for ions passage, thus enabling the generation of electrochemical gradients across the membrane, the so called "transmembrane potential (TMP)", which is crucial for example for the signal transduction along nerve cells. Nevertheless, in both medicine and biotechnology an enormous interest exists in methods that allow to transiently interrupt the membrane integrity: a reversible cell opening may enable the transfer of genes, drugs, antibodies and dyes, into the cell and may permit to trigger events by modifying the interior of the cell. There are several techniques to successfully increase the membrane permeability, but probably the most established one is the induction of pores in the lipid membrane by means of external electric fields, the technique referred to as electroporation [1,2]. Electroporation or electropermeabilization are the terms used most often to describe the cellular response to intense electric field exposure, i.e. the phenomenon of membrane increased permeability. The application of suitable electric field pulses, varying in strength and duration, permits to induce small hydrophilic pores into the membrane or tissue, thus increasing membrane permeability and allowing the transient transfer of substances into the interior of the cell [3,4]. In the past decades we assisted to the development of several applications in medicine, food processing, and biotechnology, exploited in such a large spectrum of knowledge that electroporation is now considered as a proper technological platform, including electrochemotherapy [5,6], gene electro-transfer therapy [7], calcium electroporation [8,9], tumor ablation [10,11] and food processing [12,13].

Despite this large development of techniques, the specific phenomenon underlying the transport of molecules across the cell

* Corresponding author at: Department of Information Engineering Electronic Telecommunication, Sapienza University of Rome, via Eudossiana 18, 00184 Rome, Italy.
E-mail address: francesca.apollonio@uniroma1.it (F. Apollonio).
[1] This authors equally contributed to the work.

https://doi.org/10.1016/j.bioelechem.2021.107987
1567-5394/

membrane making use of electric field pulses is complex and it involves different physical mechanisms such as: electric field dipolar coupling with bulk water [14,15], the coupling of the electric field with interfacial water [16,17], the H-bond networking in presence of intense electric fields [18,19] and the interactions between water and lipid polar heads [20-22]. As a matter of fact, there is a large variability in the molecular properties of the compounds crossing the membrane as well as in the protocols used for electroporation practice, hence an accurate description of pore formation, pore lifetimes and pore kinetics processes should be at the basis of molecular transport induced by electroporation [23,24]. In terms of experimentally determined kinetics of the process of transmembrane transport, a consensus exists that several states can be considered when dealing with the increased membrane permeability in electroporation: the initiation of the permeable state, its expansion and stabilization and the resealing of the membrane. The process can be described in terms of local lipid phase transitions which involves clusters of lipids according to a three-state scheme with a closed bilayer state, a hydrophobic pore state and a hydrophilic one [25,26]. However, the most critical aspect is the full understanding of the molecular first stage: even if the formation of aqueous pores in the lipid bilayer is now a largely accepted mechanism, there is an evidence that shows, for example, that the changes to individual membrane lipids and proteins can also contribute [27-29]. Experimental studies of the initiation of the pore are almost not practicable: this is because of their nanometer size, since the pores formed in the lipid bilayer are too small to be observed by optical microscopy, and because they are too fragile for electron microscopy's standard procedures. Even more crucial is the attempt to track the kinetics of pore initiation, where fluorescence microscopy recorded with temporal resolution has proved to be too slow [30]. Several attempts have been proposed since the last decades to support experimental pore formation with the aid of classical nucleation theory [31-33] and renewed models [34,35], explaining membrane rupture, based on defect, pre-pore and pore states, intrinsically transient and thus difficult to probe in terms of their structures and physical properties. The principal parameter to explain pore formation and pore stability of such theoretical models is the line tension, but despite its importance, line tension is still not well characterized. A further important limitation of the classical continuum models is that they neglect the molecular internal structure of membranes, hindering the transition state between the hydrophobic and the hydrophilic pores.

In the absence of experimental observation of the dynamics of pore creation, and with the limitations of continuum models, molecular dynamics (MD) simulations become an indispensable source of structural and mechanistic information. These alternative tools, giving access to the microscopic compartments of a cell on a molecular basis, provide the molecular-level evidence that the electric field promotes formation of pores in the lipid bilayers and have proven to be useful for characterizing the highly dynamic and metastable pre-pore intermediates [36,37]. Electropore formation was first demonstrated by Tieleman et al. [38], who showed the creation of a single water file defect that changed into a growing hydrophilic pore within a few ns. Consequently, several attempts have been made to fully describe the mechanism of pore creation, for which there is now general agreement that pore appears to be driven by local fast reorientation and displacement towards the membrane interior of water molecules at water/lipid interface, thus increasing the probability for defect formation [39-43]. The complete sequence presents several steps [39,44,45]: disordering of the water-membrane interface due to the applied external field which generates water defects and drives pore formation; developing of a water column penetrating the inner region of the bilayer (hydrophobic pore); reorientation of the phospholipid head groups giving rise to the hydrophilic pore. The kinetics of these states have been characterized giving rise to a model of pore formation involving initially hydrophobic pore states as short-lived transient intermediates [46,47]. An alternative approach in defining a kinetic model was provided by Bockmann and co-workers [48] who developed a statistical theory to facilitate direct comparison between experimental prepore formation kinetics and the single event preporation times, derived from the simulations. Authors suggested a model for pore formation involving a first intermediate which is characterized by a tilt of the polar lipid headgroups, and a second intermediate (prepore), where a polar chain is formed across the bilayer.

In the framework of the general theory provided in [48], in the present work we go deeper in the understanding of the molecular mechanisms at the basis of the pore formation process, providing for the first time a rationale for the definition of a consecutive first-order reaction kinetic scheme fully describing the transition among the intermediate states of the pore kinetic model. A novel methodology to derive a three-state kinetic model is proposed; this is based on the physical changes in water clusters protruding into the electropore region. The method proposed makes use of two robust biophysical quantities able to describe the system transition from the initial equilibrium condition to the pore initiation: the average number of hydrogen bonds and the number of contacts for the water molecules intruding at the water/lipid interface. The model, sustained by a robust statistical sampling, provides kinetic constants for the transition between the intact bilayer (closed state) and the finger, i.e. the metastable intermediate water filament state (hydrophobic pore state).

2. Materials and methods

2.1. Molecular dynamics simulations

MD simulations were performed using the GROMACS package, version 4.6.6 [49]. Lipid topologies were derived from the OPLS united-atom parameters [50] obtained from Peter Tieleman of the University of Calgary (http://moose.bio.ucalgary.ca). The Simple Point Charge (SPC) water model was used [51]. Systems were coupled to a temperature bath at 310 K with a relaxation time of 0.1 ps and a pressure bath at 1 bar with a relaxation time of 1 ps, each using the v-rescale coupling algorithm [52], and the Berendsen algorithm [53], respectively. Pressure was coupled semi-isotropically, using a compressibility of 4.5×10^{-5} bar^{-1} normal to and in the plane of the membrane. Bond lengths were constrained using the LINCS algorithm [54] for lipids and SETTLE [55] for water. Short-range electrostatic and Lennard-Jones interactions were cut off at 1.0 nm. Long-range electrostatics were calculated by the PME algorithm [56] using fast Fourier transforms and conductive boundary conditions. Reciprocal-space interactions were evaluated on a 0.12-nm grid with fourth-order B-spline interpolation. The parameter ewald_rtol, which controls the relative error for the Ewald sum in the direct and reciprocal space, was set to 10^{-5}. Periodic boundary conditions were employed to mitigate system size effects.

2.2. Systems and structures

All systems contained 512 lipid molecules 1-palmitoyl-2-oleoyl-*sn*-glycero-3-phosphatidylcholine (POPC) and an ionic solution made of 88 potassium ions, 88 chloride ions, and approximately 53.000 water molecules, resulting in an initial potassium-chloride concentration of about 91 mM in water. In this respect, the number of ions used in our paper was intended to reproduce the high ionic concentrations of the extracellular and intracellular media, rather than the physiological concentration of potassium

and chloride ions. Several papers suggest that such water solutions can reach 150 mM, as explained in [57] where the partial concentrations of all the main ionic species are provided. In other joint experimental/numerical *in-vitro* electroporation studies, a potassium-chloride concentration between 100 and 145 mM [23,58] was adopted. The initial box size was approximately 13 nm × 13 nm × 13 nm. Fig. 1 depicts the simulated system, highlighting the structure of the POPC leaflets.

Once the equilibrium configuration was reached (after 100 ns), extensive MD simulations have been performed: 30 independent simulations (initial velocities extracted from Maxwell-Boltzmann velocity distribution, generated from random numbers) with an external electric field with an intensity of 0.2 V/nm (see Fig. 1), applied along the positive z-axis of the Cartesian reference of frame. A second set of simulations, limited in number (10 independent simulations), were performed with a 0.17 V/nm intensity. The overall production time has exceeded ~3.5 μs.

2.3. Kinetic model

The main objective of this work is to identify, with proper tools, meaningful quantities linked to the pore creation process to fully characterize a kinetic model for pore formation. In order to tackle this, we need: i) a suitable definition for the pore initiation; ii) an objective target able to quantitatively describe the system transition from the initial equilibrium condition to the pore initiation; iii) a sufficient number of independent trials (i.e. our MD simulations) to correlate, with statistical robustness, our proposed target to the pore creation. As a basic step, we investigated the dynamics of the pore creation by choosing as the final configuration the one corresponding to the presence of a single water finger connecting the upper and lower leaflets of the lipid membrane (Fig. 2). This water finger, in principle, might reflect the partial rearrangement of lipid molecules, resulting in a tight stack of water molecules eventually forming a larger electropore. Nevertheless, as suggested by literature [59] and by our simulations results, that are explained and reported in Fig. SI-1 and Fig. SI-2 (see Section A of the Supporting Information), no meaningful lipid head rotations are found just before the water finger appearance, supporting the idea of a hydrophobic electropore in the initial stage of the poration process [34,35].

The main player of an electropore is water, which could be considered as the driver of pore formation. Hence here, we tried to link the main states associated to the pore-creation process to three specific water local behaviors. More precisely, starting from the kinetic model described in [48], we defined water initial state (see Fig. 3) as the one corresponding to the bulk-water behavior S1, the second state S2 corresponding to physical changes in water clusters protruding into the electropore region (ex-post analysis) and the final state S3 representative of the final mutual arrangement of such water molecules as a tiny water channel (i.e. finger). The transition from the water finger to the poration state (S4), where a hydrophilic sustained pore is formed, was observed in all the simulations; nevertheless, we preferred to analyze finger state formation times (S3) over pore formation times because after finger formation the effective field applied in the simulations is difficult to control, and hence pore formation is likely severely accelerated after formation of the formed finger (S3) state.

The key-role of water in defining the three-states process requires some further comments on the water model adopted and its response to an exogenous electric field. In a previous work [60], a theory linking water susceptibility and density in presence of electric field intensities within the linear response theory, has been provided. The susceptibility of pure liquid water systems has been tested comparing the available experimental [61] and simulation data (pure SPC systems at different densities) with the expected linear relation between the null field water susceptibility and density predicted by the theory. It was shown that, within the liquid range, both the experimental water data and the SPC simulated ones were fully consistent with the predicted linear behavior of water susceptibility as a function of density. Moreover, the linear regression of the experimental water data at 300 K provided slope and intercept rather close to the ones obtained by the linear regression of the corresponding simulation data of SPC at the same temperature, showing that the SPC model, within the liquid state range, reproduces reasonably well the liquid water behavior.

2.4. Water states

To describe the water behavior during the pore formation, the radial distribution function between water Oxygen atoms O_w-O_w, the g(r), has been calculated (in Fig. 4, blue line).

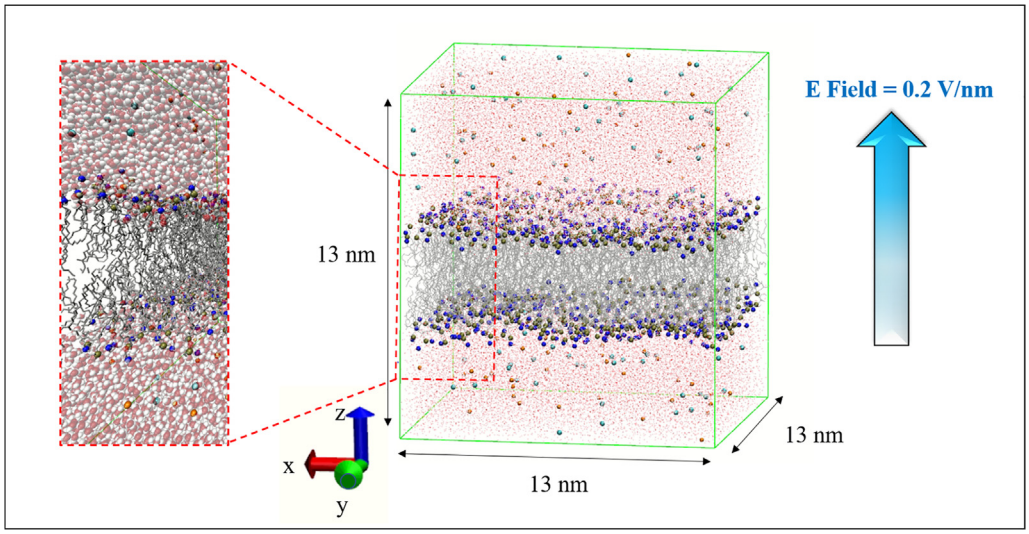

Fig. 1. Simulation box with 13x13x13 nm, composed by 512 molecules POPC (grey lines as the acyl chains and blue and tan points as P8 and N4 atoms respectively), 88 Cl^- (orange), 88 K^+ (cyan), and more than 53.000 water molecules (red and white points). A zoom of the bilayer membrane is reported as left inset. The external electric field is applied along the z-axis.

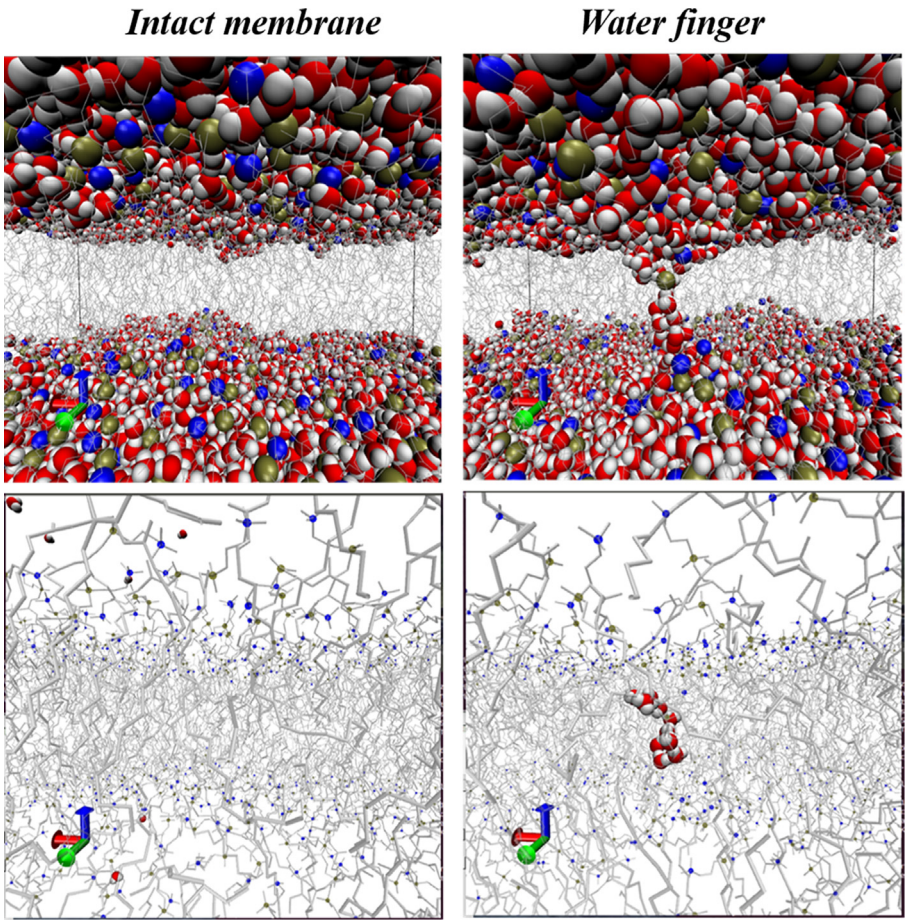

Fig. 2. Representation of the creation of a finger in the intact lipid bilayer through the identification of two states: initial state (intact bilayer) and finger state (hydrophobic pore). Upper row polar heads explicitly showed in each leaflet, lower row hydrophobic chain representing the thick of the bilayer. Grey lines represent the acyl chains and blue and tan points represent P8 and N4 atoms, respectively.

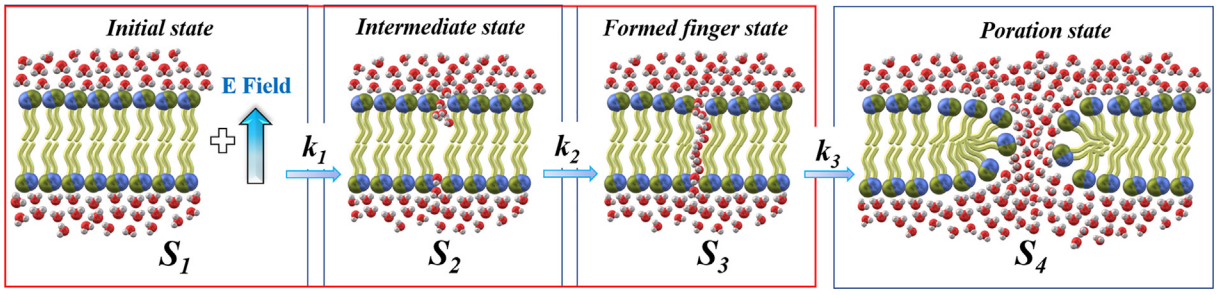

Fig. 3. Schematic 1 is a three-states Pore formation process, followed by a Schematic 2 representing the Poration state. Note that we consider the reaction irreversible.

The first peak describes the structural organization of the first hydration shell around a central O_w atom in the case of pure liquid water; in particular, the first maximum, around 0.28 nm, corresponds to the O_w-O_w average distance among the central oxygen with its nearest neighbors, while the first minimum, around 0.33 nm, corresponds to the first hydration shell radius. The coordination numbers N_c, defined as $N_c = 4\pi\rho \int_0^r r^2 g(r) dr$, were calculated by integration of the g(r) function from r = 0 nm to the distance corresponding to the first local minimum, r = 0.33 nm. This parameter provides the number of water molecules (number of contacts) in the first solvation shell around the selected O_w. As it is shown in Fig. 4 (red line), N_c = 4. These results are in agreement with the experiments in the case of liquid water [62]. It is important to stress that data reported in Fig. 4 refer to all the SPC water molecules in the simulation box. To make sure that the water molecules here considered behave as a pure water system we compared the corresponding N_c values, obtaining no meaningful differences as reported in Fig. SI-3 (see Section B of the Supporting Information).

To characterize the water dynamics, we need to identify, first, the molecules protruding in the bilayer (see Fig. 5), distinguishing them from water molecules that never will enter in the pore. To identify water molecules, we used the VMD tool [63] by means of the following procedure: starting from the finger observation, we pick 12 molecules and create an index file containing the list

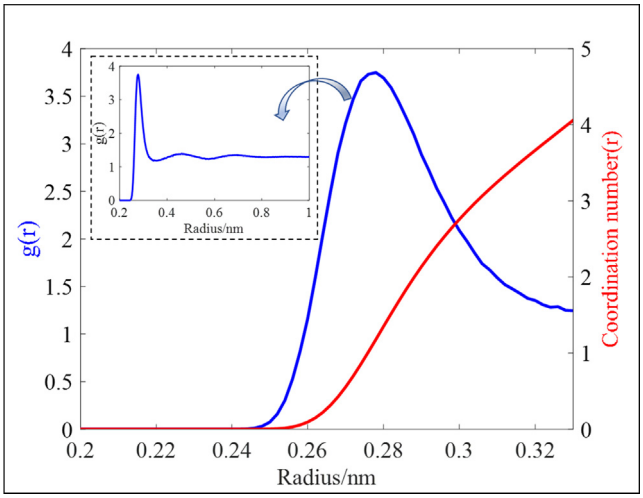

Fig. 4. The O_w-O_w water radial distribution function g(r) (in blue) and the coordination number N_c (in red) are reported. The inset represents the g(r) function profile up to 1 nm.

of the water molecules protruding in the bilayer; a second file containing the list of 12 water molecules that never will take part in the finger formation is generated as well (external water molecules).

Once the list of protruding and external water molecules is built, two quantities have been defined to characterize possible differences in the water molecule behavior. Specifically, the average number of hydrogen bonds (H_{bonds}) and the average coordination number (N_c) are studied as a function of time. This analysis has been carried out using *hbond* and *mindist* Gromacs [49] tools. The H_{bonds} are evaluated according to the following geometrical criteria: the distance among donors and acceptors is $r_{hb} \leq 0.35$ nm and the angle among donors and acceptors is $\alpha_{hb} \leq 30°$. N_c can be calculated by defining a cut-off that in our case corresponds to the first minimum of the g(r), $r_{cut\text{-}off}$ = 0.33 nm (see Fig. 4). The analysis has been performed on the complete set of simulations to demonstrate the robustness of our methodology.

2.5. Master equation

Under these circumstances, H_{bonds} and N_c turned out to be robust biophysical quantities able to describe the system transition from the initial equilibrium condition to the pore initiation. In order to capture the kinetic behavior of such sensible parameters, in principle, one needs a sufficient number of independent MD simulations in the same exposure condition, to fully characterize the stochasticity of the underlying process. As explained in [48] we modelled the time evolution of our molecular system as a probabilistic combination of three states at any given time. The switching between states is determined by two kinetic constants (see Fig. 2), leading to an overall process governed by the following equations:

$$n_1'(t) = -k_1 n_1(t) \tag{1}$$

$$n_2'(t) = k_1 n_1(t) - k_2 n_2(t) \tag{2}$$

$$n_3'(t) = k_2 n_2(t) \tag{3}$$

with solutions for the three states given by:

$$n_1(t) = e^{-k_1 t} \tag{4}$$

$$n_2(t) = \frac{k_1}{k_2 - k_1}\left(e^{-k_1 t} - e^{-k_2 t}\right) \tag{5}$$

$$n_3(t) = 1 - \left(\frac{k_2}{k_2 - k_1} e^{-k_1 t} + \frac{k_1}{k_2 - k_1} e^{-k_2 t}\right) \tag{6}$$

with n1, n2, n3 represents the population at a time t of S1, S2, S3 respectively. The validity of this model shall be confirmed wherever the three states are coherent with simulation data. This will be discussed in the following sections.

3. Results and discussion

Data obtained by the large set of 30 independent simulations in presence of the 0.2 V/nm electric pulse allowed to model the kinetics of pore formation in a meaningfully statistical way. Electric field intensity was intentionally kept high enough for the occurrence of the poration process in a reasonable time-window, but also not too high to avoid the insurgence of non-linear responses. The intensity used is at the edge of the range related to linear response theory, in fact, we implicitly consider the electric field intensity to fulfill the so-called 'weak field conditions' [18], in order to follow the process of pore formation free from parallel processes more sensible to the electric field intensity (i.e. the fast water polarization response). In

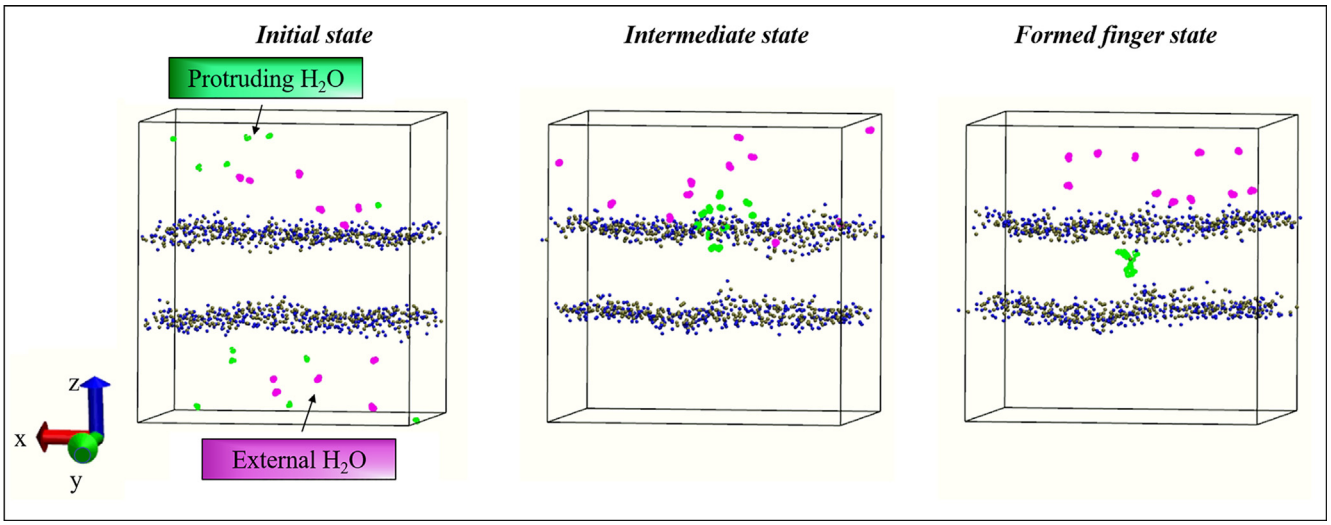

Fig. 5. Selection of water molecules used to perform the analysis: magenta points represent external H_20, green points represent protruding H_20.

the following sections we will show how protruding water dynamics (defined in the Material and Methods Section 2.4) allow a proper definition of three different water states within each independent simulation. Data obtained by a second set of 10 independent simulations with a 0.17 V/nm electric field, leading to slower poration processes while keeping the intensity below the 'weak field condition' threshold, served as evidence for the reproducibility of the proposed model. Results in terms of S2-S3 transition times are reported in Fig. SI-4, together with the related fitting curve (see Section C of the Supporting Information).

3.1. Protruding water dynamics

A representative example of H_{bonds} and N_c dynamics is reported in Fig. 6 for a single MD simulation, whereas similar results were obtained in all the simulations analyzed. The time course of H_{bonds} and N_c shown in Fig. 6 supports the behavior that those water molecules representing defects of the bilayer, hence located at the water/lipid interface (red curve), after a certain time lag (t*), have their network of hydrogen bonding disrupted by the applied field with respect to those water molecules which are part of the bulk water. This is in line with the theory of the combined effect of hydrogen bond interactions and dipole interactions in an E-field [18,64]. The idea is that water molecules at the interface sense both the external electric field applied for poration of the bilayer and the coulombic local electric field due to density charge on the lipid polar heads. This last contribution has a radial direction and is extremely fast in time evolution hence it represents a sort of spatially random stimulus, while the external applied field has a uniform direction (z-axis) and is constant in time, therefore it acts as a forcing term trying to align water molecules. The competing effects of both contributions lead to a time delay needed to break H-bonds prior to molecular rotation and new bonds can form post rotation. For bulk water molecules the only field is the one related to the external electric field hence no competing process is present and no difference in time is appreciated in the network of hydrogen bonding.

As apparent from Fig. 6, protruding and external water molecules profiles show the same behavior till a specific time, t*, when the protruding water molecules start to behave differently. Such interval is hereafter considered as the S1-S2 transition time. The time "delay" existing between t* and the instant of the finger formation (S2-S3 transitions) is extremely fast and hence challenging to characterize, but it is always present in each simulation performed.

Moreover, an additional study has been performed to evaluate the behavior of water molecules staying at the interface between the lipid bilayer and the bulk water but never taking part of the water pore, defined as interfacial water molecules. Results are reported in Fig. SI-9 (see Section E of the Supporting Information) as the time behavior of the H_{bonds} and the N_c showing that the trend, like the one of the external water molecules, is characterized by lower values without any appreciable changing at the S1-S2 transition time.

It is worth stressing that the poration process is dependent on the characteristics of the exogenous field we apply during MD simulations. Data presented in Fig. 6 reflect the general behavior of the 30 independent simulations with the 0.2 V/nm electric field. Such an intensity has been chosen as a compromise between each MD simulation production time and the number of independent simulations needed to provide robust statistics (see following Section 3.2). Moreover, exogenous electric fields lower than a certain threshold [36] can't produce poration events within an acceptable time window (100 ns). At the same time, electric fields higher than 0.2 V/nm could mean stepping outside the limitations of the Linear Response Theory [64], which implies an unrealistic water polarization response. Nonetheless, to give evidence that the profiles given in Fig. 6 represent an intensity-independent result, we analyzed results coming from 10 MD simulations with an intensity of 0.17 V/nm. In this case, apart from a change in kinetics constants values (the finger formation event can take place after 200 ns), all data suggest that the H_{bonds} and N_c still conveniently interpret the 3-states kinetic model, as expected (data shown in Section C of the Supporting Information).

To test the validity of the two physical quantities chosen to define water states, we evaluated the polarization response of the protruding water molecules in time. In fact, H_{bonds} and N_c decrease could be a consequence of a much faster process such as water polarization response [18]. Fig. 7 shows the time-course of the total dipole moment of both external and protruding water molecules, evidencing no appreciable differences for the whole dynamics, particularly after the time frame t*.

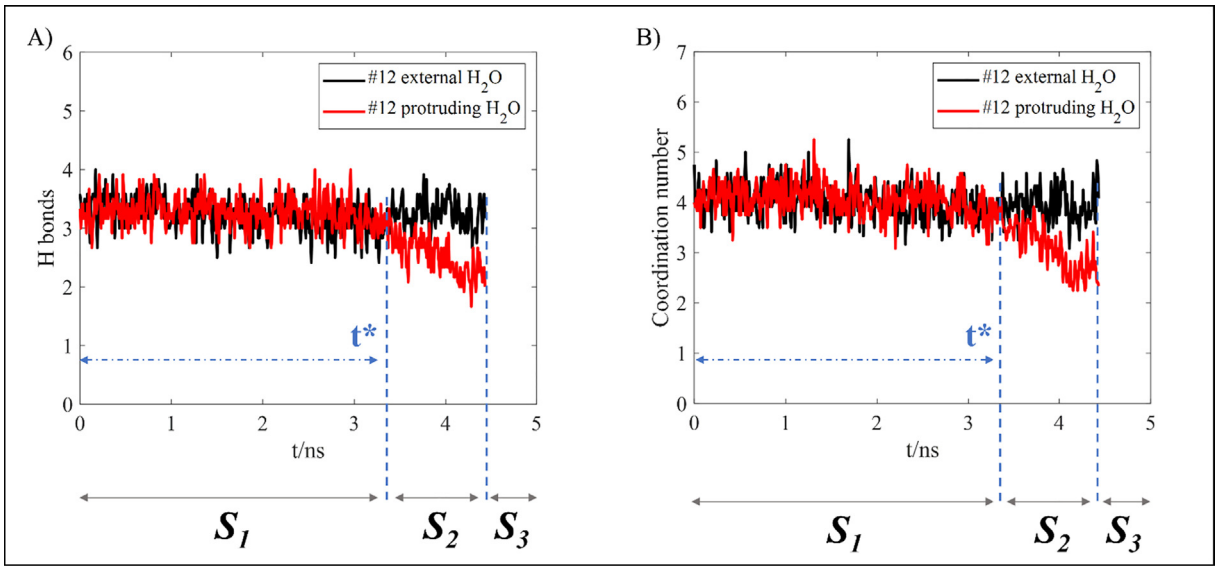

Fig. 6. The H_{bonds} and N_c are reported in case of protruding water molecules (red) and external water molecules (black) along the simulation time.

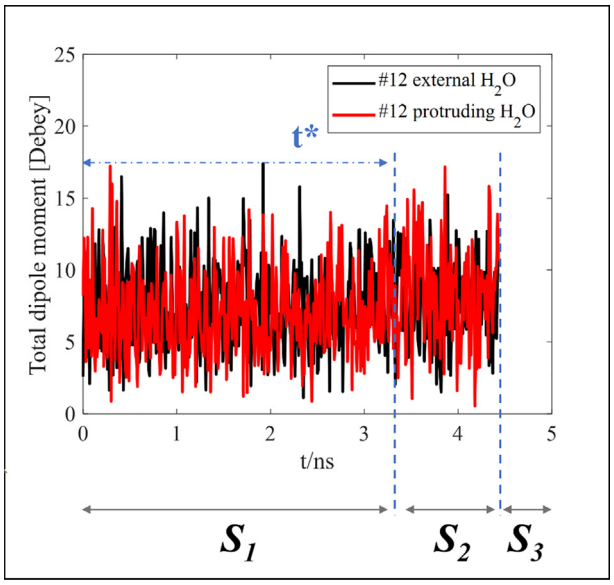

Fig. 7. Time-course of the total dipole moment of protruding (red) and (black) external water molecules, evaluated for the same sample simulation used for H_{bonds} and N_c dynamics evaluation.

Similar results were obtained for all simulations (in the two different exposure conditions), as can be seen in Section D of the Supporting Information, where more simulations outcomes are reported in terms of H_{bonds}, N_c and total dipole moment (Fig. SI-5, SI-6, SI-7 for the 0.2 V/nm intensity).

3.2. Link with the kinetic model

Transition times from state S1 to S2 and overall transition times from state S1 to state S3 are reported, for the 0.2 V/nm intensity, in Table SI-I (see details in Section F of the Supporting Information). These results are in line with similar ones available in the literature, where poration times are reported for different lipid composition in [65] as well as for different intensities ranging from 0.05 V/nm up to 0.2 V/nm in [36]. Data shown highlight the randomness of the pore creation process.

Fig. 8 reports the data of Table SI-I as three cumulative sums over time, where each sum represents a distinct (state) population: i) green points are associated with S1 population disappearance, during the transition towards S2. Points range from 1 (i.e. S1 is fully populated) down to 0, when the transition toward S2 is complete; ii) red points represent the population of the final state S3 and it ranges from 0 (no porating event) to 1 (all the simulation ended up with a poration event); iii) the blue points represent the intermediate state S2, to whom or from whom the populations of S1 and S3 states, respectively, are transferred. As apparent from the data, the profile of the intermediate state, while suggesting a clear profile, would take a benefit from an even larger number of simulations with respect to the ones chosen here as the necessary trade-off with a computationally expensive approach as MD simulations (more than 3.5 μs simulation time). Remarkably, data fitted with the set of Eqs. (4)–(6) indicate that the model can capture the essence of the pore formation process. In particular, MATLAB R2020b [66] was used to solve the nonlinear curve-fitting (data-fitting) problems in least-squares sense, providing a residual matrix with single values ranging from 0.005 to 0.12 as reported in Table SI-II (see details in Section F of the Supporting Information).

Note that the S1-S2 transition is usually much slower than the S2-S3 transition. Also, while the S1-S2 transition has a large variability in time durations, as soon as the process reaches the S2 state the transition time toward S3 state is rather constant. Overall, the fastest appearance of the water finger takes place after about 4 ns from the electric field application, while the slowest one takes place after more than 40 ns from the electric field switched on. The mean time intervals associated to S1-S2 and S2-S3 transitions can be obtained by the inverse of the kinetic constants k_1 and k_2 found during the fitting procedure. Simple calculations furnish for $\tau_1 = k_T^{-1} = 13.05$ ns and for $\tau_2 = k_2^{-1} = 1.4$ ns; that is the S2-S3 transition results about 10 times faster than the S1-S2 one.

But here a question arises: which is the minimum number of data needed to provide a robust output for our model? To this purpose, we evaluated the statistics of our outcomes in the following way: i) starting from the complete set of 30 simulation with the 0.2 V/nm intensity, we considered an increasing number of MD simulation sub-sets, i.e. 5, 10, 12, 17, 20, 25 and 30, randomly extracted within the total population; ii) we calculated the kinetics parameters, as given by the three-states model, for the previous MD simulation sets; iii) we evaluated the ratio k_1/k_2 at increasing MD simulation population. The result of such approach is a convergence plot as shown in Fig. 9, highlighting that a minimum number of 10 MD simulation is needed to start to stabilize the k_1/k_2 profile (for more details see Table SI-III in Section G of the Supporting Information), while a larger set of at least 20 MD simulations is needed to have a fully convergence. Note that, when considering the smallest 5 MD simulations set, the k_1/k_2 ratio is almost twice the most populated sets, meaning that a particular caution should be used to give a statistical robustness to such kinetic studies.

For this reason, the description of the three states S1-S2-S3 is fully provided just for the large simulation set at 0.2 V/nm; the simulations at 0.17 V/nm evidence a similar k_1/k_2 ratio and a good consistency with the kinetic model (see Section C of the Supporting Information), but the limited number of independent processes (due to the large computational cost) limits the robustness of the approach.

3.3. Validity and limitation of the present approach

As a corollary to the above discussion, it should be stressed that the previous kinetic model has been obtained for two sets of simulations, the first one with a 0.2 V/nm electric field and the second one with a 0.17 V/nm electric field. Motivations for such a choice refer to the search of the very basic mechanisms of interaction between the external field and the main characters leading to pore initiation, i.e. water molecules, hard to describe with higher intensity electric fields. As an example, in the work by Bockmann et al. [48] pore formation has been observed with electric field strengths ranging from 0.36 to 0.70 V/nm, obtaining (logarithmic) pore formation times, determined as the time span between onset of the electric field and observation of the first closed water/lipid file across the membrane core. Bockmann et al. [48] assumed one main activation barrier to describe pore formation times with the change in the average activation dipole moment upon the pore formation event.

With our methodology, while confirming the expected polarization response of water molecules with the intensities used, we could not discriminate between bulk water (named external water in Material and Methods, Section 2.4) and protruding water behavior in terms of polarization, since no appreciable dipole difference emerged between the two species for the entire pore formation process (for the complete set of analyzed trajectories). On the other hand, the specific quantities we have chosen, i.e. H_{bonds} and N_c dynamics, allowed to capture the polarization-independent response of both bulk and protruding water, showing that a change in water interaction behavior could be the fingerprint for identifying the intermediate state in the kinetic process of pore formation. Moreover, the use of an electric field which is near the threshold for the linear response theory, ensures a reliable characterization

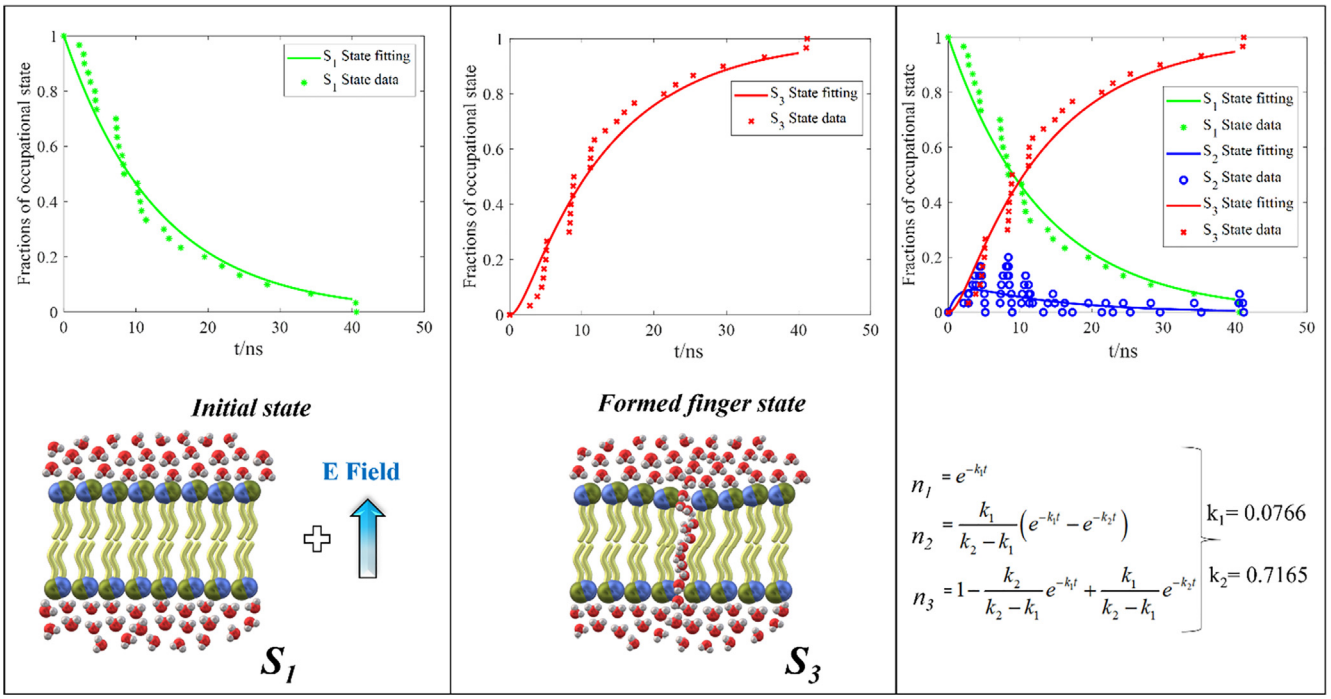

Fig. 8. Each color group represents a specific water state: green, blue and red points represent S1, S2 and S3 states populations, respectively. Colored curves represent the fitting of numerical data with the equation furnished by the kinetic model.

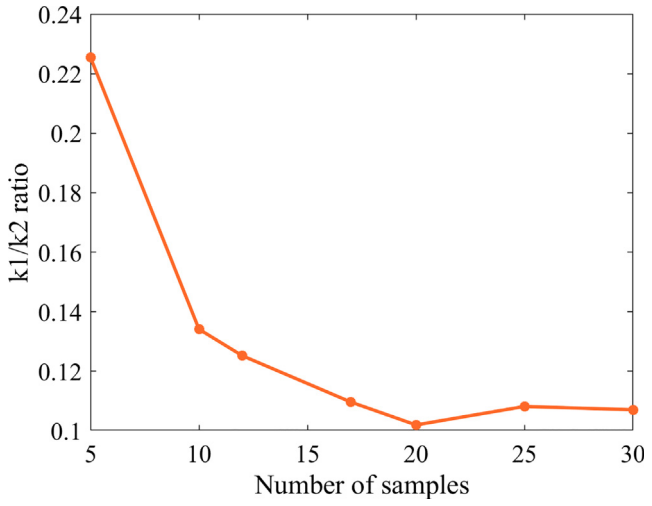

Fig. 9. The ratio between the k1 and k2 kinetics parameters are reported as a function of the number of simulation samples considered.

of such physical quantities, which would otherwise be overtaken with higher intensity electric fields. To support this assumption, we performed three sets of simulations (10 simulation per set) with electric fields ranging from 0.3 V/nm up to 0.5 V/nm, finding that the polarization response with such high intense electric field completely overlooks the H_{bonds} and N_c dynamics, as shown in Fig. SI-8 (see section D of the Supporting Information), also hiding the presence of the S2 intermediate state as defined in our kinetic model.

4. Conclusions

The numerical exploration, via MD simulations, of the kinetics of electroporation led to the construction of solid schemes [45] capable of dividing the whole process into different states, using the time evolution populations of water and phospholipid head groups as indicators of the specific conformational state. The transitions between these states have been studied by Bockmann and coworkers [48] who developed a statistical theory to facilitate a direct comparison between experimental (macroscopic) prepore formation kinetics and the (single event) preporation times derived from the simulations. Authors suggested a model for pore formation governed by the polarization response of both water molecules and lipids.

Here we focused on the initial electroporation steps, i.e. the transition from the initial intact double-layer to the appearance of a tight stack of water molecules, eventually able to form a larger electropore, usually named water-finger. Within our simulation procedure we observed no meaningful lipid head rotations just before the water finger appearance, supporting the idea of a hydrophobic electropore in the initial stage of the process of poration [34,35]. Hence, we identified water as the main player of pore formation: in particular, we defined water initial state as the one corresponding to the bulk-water behavior, the second state corresponding to physical changes in water clusters protruding into the bilayer (ex-post analysis) and the final state representative of the final mutual arrangement of such water molecules as pillar of the water finger.

The methodology that we developed to follow water dynamical transition during the whole process of pore formation, allowed to go deeper in the understanding of the molecular mechanisms involved in such a process, providing for the first time a rationale for the definition of a consecutive first-order kinetic scheme fully describing the transition among the intermediate states of the pore kinetic model. Here authors present a three-state kinetic model for the process of pore creation based on the assessed mechanism of water defects intruding at the water/lipid interface as obtained for electric field intensities in the edge of the linear regime. The model proposed, sustained by a robust statistical sampling, provides kinetic constants for the transition between the intact bilayer (closed state) and the finger, i.e. the metastable intermediate water filament state (hydrophobic pore state).

Declaration of Competing Interest

The authors declare that they have no known competing financial interests or personal relationships that could have appeared to influence the work reported in this paper.

Acknowledgments

Francesca Apollonio acknowledges financial support from the Sapienza University of Rome, Research Projects, 2019 (No. RM11916B835D12D4).

Micaela Liberti acknowledges financial support from the Sapienza University of Rome, Research Projects, 2017 (No. RM11715C7DCB8473).

Appendix A. Supplementary material

Supplementary data to this article can be found online at https://doi.org/10.1016/j.bioelechem.2021.107987.

References

[1] J.C. Weaver, Y.A. Chizmadzhev, Theory of electroporation: a review, Bioelectrochem. Bioenerg. 41 (1996) 135–160, https://doi.org/10.1016/S0302-4598(96)05062-312.
[2] J. Teissie, Mechanistic description of membrane electropermeabilization, in: D. Miklavčič (Ed.), Handbook of Electroporation, Springer, Cham, 2017, https://doi.org/10.1007/978-3-319-328867_39.
[3] L. Rems, Lipid pores: molecular and continuum models, in: D. Miklavčič (Ed.), Handbook of Electroporation, Springer International Publishing, Cham, 2017, pp. 3–23, https://doi.org/10.1007/978-3-319-32886-7_76.
[4] T. Kotnik, L. Rems, M. Tarek, D. Miklavčič, Membrane electroporation and electropermeabilization: mechanisms and models, Annu. Rev. Biophys. 48 (1) (2019) 63–91.
[5] M. Marty, G. Sersa, J.R. Garbay, J. Gehl, C.G. Collins, M. Snoj, V. Billard, P.F. Geertsen, J.O. Larkin, D. Miklavcic, I. Pavlovic, S.M. Paulin-Kosir, M. Cemazar, N. Morsli, D.M. Soden, Z. Rudolf, C. Robert, G.C. O'Sullivan, L.M. Mir, Electrochemotherapy–an easy, highly effective and safe treatment of cutaneous and subcutaneous metastases: results of ESOPE (European standard operating procedures of Electrochemotherapy) study, Eur. J. Cancer Suppl. 4 (11) (2006) 3–13.
[6] A. Gothelf, L.M. Mir, J. Gehl, Electrochemotherapy: results of cancer treatment using enhanced delivery of bleomycin by electroporation, Cancer Treat. Rev. 29 (5) (2003) 371–387.
[7] A.I. Daud, R.C. DeConti, S. Andrews, P. Urbas, A.I. Riker, V.K. Sondak, P.N. Munster, D.M. Sullivan, K.E. Ugen, J.L. Messina, R. Heller, Phase I trial of interleukin-12 plasmid electroporation in patients with metastatic melanoma, J. Clin. Oncol. 26 (36) (2008) 5896–5903.
[8] S.K. Frandsen, M.B. Krüger, U.M. Mangalanathan, T. Tramm, F. Mahmood, I. Novak, J. Gehl, Normal and malignant cells exhibit differential responses to calcium electroporation, Cancer Res. 77 (16) (2017) 4389–4401.
[9] H. Falk, S. Lambaa, H.H. Johannesen, G. Wooler, A. Venzo, J. Gehl, Electrochemotherapy and calcium electroporation inducing a systemic immune response with local and distant remission of tumors in a patient with malignant melanoma – a case report, Acta Oncol (Madr). 56 (8) (2017) 1126–1131.
[10] R.V. Davalos, L.M. Mir, B. Rubinsky, Tissue ablation with irreversible electroporation, Ann. Biomed. Eng. 33 (2) (2005) 223–231.
[11] R. Nuccitelli, A. McDaniel, S. Anand, J. Cha, Z. Mallon, J.C. Berridge, D. Uecker, Nano-Pulse Stimulation is a physical modality that can trigger immunogenic tumor cell death, J. ImmunoTher. Cancer 5 (1) (2017), https://doi.org/10.1186/s40425-017-0234-5.
[12] K. Dymek, P. Dejmek, F.G. Galindo, Influence of pulsed electric field protocols on the reversible Permeabilization of Rucola leaves, Food Bioprocess Technol. 7 (3) (2014) 761–773.
[13] M. Sack, J. Sigler, S. Frenzel, C. Eing, J. Arnold, T. Michelberger, W. Frey, F. Attmann, L. Stukenbrock, G. Müller, Research on industrial-scale electroporation devices fostering the extraction of substances from biological tissue, Food Eng. Rev. 2 (2010) 147–156.
[14] A. Baer, Z. Miličević, D.M. Smith, A.-S. Smith, Water in an electric field does not dance alone: the relation between equilibrium structure, time dependent viscosity and molecular motions, J. Mol. Liq. 282 (2019) 303–315.
[15] G. Sutmann, Structure formation and dynamics of water in strong external electric fields, J. Electroanal. Chem. 450 (2) (1998) 289–302.
[16] E.A. Disalvo, F. Lairion, F. Martini, E. Tymczyszyn, M. Frías, H. Almaleck, G.J. Gordillo, Structural and functional properties of hydration and confined water in membrane interfaces, Biochimica Biophysica Acta – Biomembr. 1778 (12) (2008) 2655–2670.
[17] P. Stevenson, A. Tokmakoff, Ultrafast fluctuations of high amplitude electric fields in lipid membranes, J. Am. Chem. Soc. 139 (13) (2017) 4743–4752.
[18] S.J. Suresh, A.V. Satish, A. Choudhary, Influence of electric field on the hydrogen bond network of water, J. Chem. Phys. 124 (7) (2006 Feb 21) 74506, https://doi.org/10.1063/1.2162888.
[19] H. Elgabarty, N.K. Kaliannan, T.D. Kühne, Enhancement of the local asymmetry in the hydrogen bond network of liquid water by an ultrafast electric field pulse, Sci. Rep. 9 (1) (2019) 10002.
[20] P.T. Vernier, Z.A. Levine, M.-C. Ho, S. Xiao, I. Semenov, A.G. Pakhomov, Picosecond and terahertz perturbation of interfacial water and electropermeabilization of biological membranes, J. Membr. Biol. 248 (5) (2015) 837–847.
[21] J. Tang, J. Ma, L. Guo, K. Wang, Y. Yang, W. Bo, L. Yang, Z. Wang, H. Jiang, Z. Wu, B. Zeng, Y. Gong, Interpretation of the molecular mechanism of the electroporation induced by symmetrical bipolar picosecond pulse trains, Biochimica Biophysica Acta – Biomembr. 1862 (5) (2020) 183213.
[22] F. Martelli, C. Calero, G. Franzese, Redefining the concept of hydration water near soft interfaces, Biointerphases 16 (2) (2021) 020801.
[23] E.B. Sözer, C.F. Pocetti, P.T. Vernier, Transport of charged small molecules after electropermeabilization - drift and diffusion, BMC Biophysics 11 (1) (2018), https://doi.org/10.1186/s13628-018-0044-2.
[24] T. Kotnik, G. Pucihar, D. Miklavčič, Induced transmembrane voltage and its correlation with electroporation- mediated molecular transport, J. Membr. Biol. 236 (1) (2010) 3–13.
[25] S. Kakorin, S.P. Stoylov, E. Neumann, Electro-optics of membrane electroporation in diphenylhexatriene-doped lipid bilayer vesicles, Biophys. Chem. 58 (1-2) (1996) 109–116.
[26] K.C. Melikov, V.A. Frolov, A. Shcherbakov, A.V. Samsonov, Y.A. Chizmadzhev, L.V. Chernomordik, Voltage-induced nonconductive pre-pores and metastable single pores in unmodified planar lipid bilayer, Biophys. J. 80 (4) (2001) 1829–1836.
[27] L. Rems, M.A. Kasimova, I. Testa, L. Delemotte, Pulsed electric fields can create pores in the voltage sensors of voltage-gated ion channels, Biophys. J. 119 (1) (2020) 190–205, https://doi.org/10.1016/j.bpj.2020.05.030.
[28] M. Bernardi, P. Marracino, M.R. Ghaani, M. Liberti, F. Del Signore, C.J. Burnham, J.-A. Gárate, F. Apollonio, N.J. English, Human aquaporin 4 gating dynamics under axially oriented electric-field impulses: a non-equilibrium molecular-dynamics study, J. Chem. Phys. 149 (24) (2018), https://doi.org/10.1063/1.5044665 245102.
[29] P. Marracino, M. Bernardi, M. Liberti, F. Del Signore, E. Trapani, J.A. Gárate, C.J. Burnham, F. Apollonio, N.J. English, Transprotein-electropore characterization: a molecular dynamics investigation on human AQP4, ACS Omega 3 (11) (2018) 15361–15369, https://doi.org/10.1021/acsomega.8b02230.
[30] J.T. Sengel, M.I. Wallace, Imaging the dynamics of individual electropores, Proc. Natl. Acad. Sci. 113 (19) (2016) 5281–5286, https://doi.org/10.1073/pnas.1517437113.
[31] I.G. Abidor, V.B. Arakelyan, L.V. Chernomordik, Y.A. Chizmadzhev, V.F. Pastushenko, M.R. Tarasevich, Electric breakdown of bilayer lipid membranes I. The main experimental facts and their qualitative discussion, Bioelectrochem. Bioenerg. 6 (1979) 37–52, https://doi.org/10.1016/0302-4598(79)85005-9.
[32] R.W. Glaser, S.L. Leikin, L.V. Chernomordik, V.F. Pastushenko, A.I. Sokirko, Reversible electrical breakdown of lipid bilayers: formation and evolution of pores, Biochim. Biophys. Acta, Biomembr. 940 (2) (1988) 275–287, https://doi.org/10.1016/0005-2736(88)90202-7.
[33] J.C. Weaver, Y.A. Chizmadzhev, Theory of electroporation: a review, Bioelectrochem. Bioenerg. 41 (2) (1996) 135–160, https://doi.org/10.1016/S0302-4598(96)05062-3.
[34] S.A. Akimov, P.E. Volynsky, T.R. Galimzyanov, P.I. Kuzmin, K.V. Pavlov, O.V. Batishchev, Pore formation in lipid membrane I: Continuous reversible trajectory from intact bilayer through hydrophobic defect to transversal pore, Sci. Rep. 7 (1) (2017) 12152, https://doi.org/10.1038/s41598-017-12127-7.
[35] S.A. Akimov, P.E. Volynsky, T.R. Galimzyanov, P.I. Kuzmin, K.V. Pavlov, O.V. Batishchev, Pore formation in lipid membrane II: Energy landscape under external stress, Sci. Rep. 7 (1) (2017) 12509, https://doi.org/10.1038/s41598-017-12749-x.
[36] M.L. Fernández, M. Risk, R. Reigada, P.T. Vernier, Size-controlled nanopores in lipid membranes with stabilizing electric fields, Biochem. Biophys. Res. Commun. 423 (2) (2012) 325–330, https://doi.org/10.1016/j.bbrc.2012.05.122.
[37] F. Dehez, L. Delemotte, P. Kramar, D. Miklavčič, M. Tarek, Evidence of conducting hydrophobic nanopores across membranes in response to an electric field, J. Phys. Chem. C 118 (13) (2014) 6752–6757, https://doi.org/10.1021/jp4114865.
[38] D.P. Tieleman, The molecular basis of electroporation, BMC Biochem. 5 (2004) 1–12, https://doi.org/10.1186/1471-2091-5-10.
[39] M. Tokman, J.H. Lee, Z.A. Levine, M.-C. Ho, M.E. Colvin, P.T. Vernier, J.M. Sanchez-Ruiz, Electric field-driven water dipoles: nanoscale architecture of electroporation, PLoS ONE 8 (4) (2013) e61111, https://doi.org/10.1371/journal.pone.0061111.
[40] P.T. Vernier, M.J. Ziegler, Nanosecond field alignment of head group and water dipoles in electroporating phospholipid bilayers, J. Phys. Chem. B 111 (45) (2007) 12993–12996, https://doi.org/10.1021/jp077148q.
[41] M. Tarek, Membrane electroporation: a molecular dynamics simulation, Biophys. J. 88 (6) (2005) 4045–4053, https://doi.org/10.1529/biophysj.104.050617.

[42] A.A. Gurtovenko, J. Anwar, I. Vattulainen, Defect-mediated trafficking across cell membranes: insights from in silico modeling, Chem. Rev. 110 (10) (2010) 6077–6103, https://doi.org/10.1021/cr1000783.
[43] S.A. Kirsch, R.A. Böckmann, Membrane pore formation in atomistic and coarse-grained simulations, Biochimica Biophysica Acta – Biomembr. 10 (1858) 2266–2277.
[44] M.L. Fernández, G. Marshall, F. Sagués, R. Reigada, Structural and kinetic molecular dynamics study of electroporation in cholesterol-containing bilayers, J. Phys. Chem. B 114 (20) (2010) 6855–6865, https://doi.org/10.1021/jp911605b.
[45] Z.A. Levine, P.T. Vernier, Life cycle of an electropore: Field-dependent and field independent steps in pore creation and annihilation, J. Membr. Biol. 236 (1) (2010) 27–36, https://doi.org/10.1007/s00232-010-9277-y.
[46] E. Neumann, S. Kakorin, Membrane electroporation: chemical thermodynamics and flux kinetics revisited and refined, Eur. Biophys. J. 47 (4) (2018) 373–387, https://doi.org/10.1007/s00249-018-1305-3.
[47] I.P. Sugar, E. Neumann, Stochastic model for electric field-induced membrane pores, Electroporation. Biophys. Chem. 19 (3) (1984) 211–225, https://doi.org/10.1016/0301-4622(84)87003-9.
[48] R.A. Böckmann, B.L. De Groot, S. Kakorin, E. Neumann, H. Grubmüller, Kinetics, statistics, and energetics of lipid membrane electroporation studied by molecular dynamics simulations, Biophys. J. 95 (4) (2008) 1837–1850, https://doi.org/10.1529/biophysj.108.129437D.
[49] D. van der Spoel, E. Lindahl, B. Hess, the GROMACS development team, GROMACS User Manual version 4.6.6, www.gromacs.org, 2014.
[50] O. Berger, O. Edholm, F. Jähnig, Molecular dynamics simulations of a fluid bilayer of dipalmitoylphosphatidylcholine at full hydration, constant pressure, and constant temperature, Biophys. J. 72 (5) (1997) 2002–2013, https://doi.org/10.1016/S0006-3495(97)78845-3.
[51] H.J.C. Berendsen, J.P.M. Postma, W.F. van Gunsteren, J. Hermans, Interaction models of water in relation to protein hydration, in: B. Pullman (Ed.) Intermolecular forces: Proceedings of the Fourteenth Jerusalem Symposium on Quantum Chemistry and Biochemistry, vol. 14, Reidel Publ. Company, Dordrecht, Holland, pp. 331–342.
[52] G. Bussi, D. Donadio, M. Parrinello, Canonical sampling through velocity rescaling, J. Chem. Phys. 126 (1) (2007) 014101, https://doi.org/10.1063/1.2408420.
[53] H.J.C. Berendsen, J.P.M. Postma, W.F. Van Gunsteren, A. Dinola, J.R. Haak, Molecular dynamics with coupling to an external bath, J. Chem. Phys. 81 (8) (1984) 3684–3690, https://doi.org/10.1063/1.448118.
[54] B. Hess, H. Bekker, H.J.C. Berendsen, J.G.E.M. Fraaije, LINCS: a linear constraint solver for molecular simulations, J. Comput. Chem. 18 (12) (1997) 1463–1472, https://doi.org/10.1002/(SICI)1096-987X(199709)18:12<1463::AID-JCC4>3.0.CO;2-H.
[55] S. Miyamoto, P.A. Kollman, SETTLE: an analytical version of the SHAKE and RATTLE algorithm for rigid water, Models. 13 (8) (1992) 952–962, https://doi.org/10.1002/jcc.540130805.
[56] U. Essmann, L. Perera, M.L. Berkowitz, T. Darden, H. Lee, L.G. Pedersen, A smooth particle mesh Ewald method, J. Chem. Phys. 103 (19) (1995) 8577–8593, https://doi.org/10.1063/1.470117.
[57] C. Merla, A.G. Pakhomov, I. Semenov, P.T. Vernier, Frequency spectrum of induced transmembrane potential and permeabilization efficacy of bipolar electric pulses, Biochimica Biophysica Acta – Biomembr. 1859 (7) (2017) 1282–1290, https://doi.org/10.1016/j.bbamem.2017.04.014.
[58] E.B. Sözer, S. Haldar, P.S. Blank, F. Castellani, P.T. Vernier, J. Zimmerberg, Dye transport through bilayers agrees with lipid electropore molecular dynamics, Biophys. J. 119 (9) (2020) 1724–1734, https://doi.org/10.1016/j.bpj.2020.09.028.
[59] M.J. Ziegler, P. Thomas Vernier, Interface water dynamics and porating electric fields for phospholipid bilayers, J. Phys. Chem. B 112 (43) (2008) 13588–13596, https://doi.org/10.1021/jp8027726.
[60] A. Amadei, P. Marracino, Theoretical-computational modelling of the electric field effects on protein unfolding thermodynamics (2015), RSC Adv. 5 (117) (2015) 96551–96561.
[61] M. Uematsu, E.U. Frank, Static dielectric constant of water and steam, J. Phys. Chem. Ref. Data 9 (4) (1980) 1291–1306, https://doi.org/10.1063/1.555632.
[62] A.K. Soper, M.G. Phillips, A new determination of the structure of water at 25°C, Chem. Phys. 107 (1) (1986) 47–60, https://doi.org/10.1016/0301-0104(86)85058-3.
[63] W. Humphrey, A. Dalke, K. Schulten, VMD - visual molecular dynamics, J. Molec. Graphics 14 (1996) 33–38, http://www.ks.uiuc.edu/Research/vmd/.
[64] P. Marracino, M. Liberti, G. d'Inzeo, F. Apollonio, Water response to intense electric fields: a molecular dynamics study, Bioelectromagnetics 36 (5) (2015) 377–385, https://doi.org/10.1002/bem.21916.
[65] M. Casciola, D. Bonhenry, M. Liberti, F. Apollonio, M. Tarek, A molecular dynamic study of cholesterol rich lipid membranes: Comparison of electroporation protocols, Bioelectrochemistry 100 (2014) 11–17, https://doi.org/10.1016/j.bioelechem.2014.03.009.
[66] The Math Works, Inc. MATLAB. Version 2020b, The Math Works, Inc., 2020. Computer Software. www.mathworks.com/.

Paolo Marracino obtained his PhD in Electronic Engineering at the University of Rome "La Sapienza" in 2010 and until September 2017, as post-doc, he focused on the study of interaction mechanisms between EM fields and biological systems at the microscopic level, including molecular dynamics simulations and the design and manufacture of systems for real-time EM field exposures. Since September 2017 he works for RISE Technology Srl as researcher for innovative biomedical devices.

Laura Caramazza received a master degree (cum laude) in Nanotechnology Engineering at Sapienza University of Rome in 2018.Presently she is at the end of the third year of the PhD in Information and Communications Technologies (curriculum Electronic Engineering), at Sapienza University of Rome and supported by the Center for Life Nano- & Neuro-Science of Istituto Italiano di Tecnologia (IIT), Rome, Italy. Her research topic is focused on the study of drug delivery systems activated by electric and magnetic fields. She has an active part in the collaboration with the Department of Drug Chemistry of Sapienza University. She worked at the CNRS - University of Paris-Saclay - Gustave Roussy UMR 9018, METSY, Paris, France during her Short Term Mission as Grant winner for the project "Investigations on driving mechanisms of lipid vesicles destabilization due to intense electric fields with characteristics of the lightning" in the framework of the COST Action [CA15211] ElectroNET.

Maria Montagna got her master degree in Physics at the Univ. of Rome La Sapienza (Italy). In 2014, she got her PhD in Engineering and Physical-Mathematical Modeling at University of L'Aquila, (Italy). Later, she worked as postdoc in different institutions in Italy and Germany; the main interests of her scientific career are devoted to biophysics, nanotechnology and material science using a computational modeling approach. From August 2020 she joined Prof. D'Inzeo group at Dep. Engineering of Rome La Sapienza to study the effect of electric field on biomolecules by means of molecular dynamics simulations

Ramin Ghahri received his bachelor's degree in electronics engineering from Razi University of Iran in 2014, he received an admission for master's degree in Nanotechnology Engineering at Sapienza University of Rome, Italy. He is currently writing his master's degree thesis on electroporation of lipid bilayers with molecular dynamics simulations. He is involved in research on kinetics of pore formation in lipid membranes as well as electroporation of POPE membranes. His research interests include electroporation, biomedical engineering, biosensors, drug delivery, bio electrics, photonics, optics, plasmonics, nano particles and condensed matter physics. His current research interests include a molecular dynamics investigation on POPC and POPE lipid bilayers, electroporation of biological membranes for biomedical applications.

Marco D'Abramo received his Master Degree in Chemistry in 2003 and his PhD in Chemical Sciences in 2007 with a thesis entitled "Statistical mechanical modelling of complex systems: thermodynamics and electronic properties". He spent two years as a post-doctoral fellow in Barcelona (Universidad de Barcelona and Institute of Research in Biomedicine) in the group of Modesto Orozco. He moved to Madrid (Spanish National Cancer Research Center) in 2010. From 2013 to 2014 was Head of the Computational Unit @ CINECA (Italy). In 2014 he obtained a tenure-track position at the Chemistry Dept. of Sapienza University of Rome, where in April, 2017 he became Associate Professor in Physical Chemistry. Marco D'Abramo is co-author of about 55 publications in international peer-reviewed journals and he has several international collaborations with theoretical and experimental scientists in the Physical Chemistry and Biophysics field of research.

Micaela Liberti, received the M.Sc degree in Electronic Engineering and doctorate degree from Sapienza University of Rome, Italy in 1995 and 2000, respectively. She is currently Associate Professor with the Department of Electronic Engineering, Sapienza University. Presently she is the President of the European Bioelectromagnetic Association (EBEA) that she joined as Scientific Council member first and Secretary afterwards since 2008. From 2018 to 2019 she has been Technical Program Committee Chair of the Bioelectromagnetics Conference. Since 2018 she is Associate Editor in the editorial board of the IEEE Journal of Electromagnetics, RF and Microwaves in Medicine and Biology, and since 2016 she acts as Review Editor for Frontiers in Public Health–Radiation and Health. From 2012 to 2015, she served as the national supplent representative of COST TD1104: "European network for development of electroporation-based technologies and treatments". From 2008 to 2012 she has been Expert Member in the Coordinated Action COST BM0704 "Emerging EMF Technologies Health Risk Management" and from 2004 to 2008 she has been Expert Member of the Technical Working Groups in the EMF-NET "Effects of the exposure to electromagnetic fields: From science to public health and safer workplace", 6th Framework Program. Her scientific interests include theoretical modeling in bioelectromagnetics, microdosimetry, exposure systems dosimetry and design, biomedical applications of EM fields, electroporation.

Francesca Apollonio (M'06) received the Doctorate degree from the Sapienza University of Rome, Rome, Italy, 1998. Since 2000, she joined the Department of Electronic Engineering, Sapienza University of Rome as Assistant Professor and since 2019 she is Associate Professor. Presently she is Chair of the National Commission CNR-URSI, Commission K "Electromagnetics in Biology and Medicine", while she has been member of the same Commission since 2011. Since 2016 she has been National Representative for the Action COST CA15211: "Atmospheric Electricity Network: coupling with the Earth System, climate and biological systems" (Electronet). From 2012 to 2015, she served on the Board of Directors of the Bioelectromagnetic Society. In 2015-2016 she has been Chair of the TPC (Technical Program Committee) for the Annual Meeting of the Bioelectromagnetics Society (BEMS) and the European BioElectromagnetics Association (EBEA), BioEM2016 held in Ghent, Belgium. Her research interests include the main aspects related to the interaction between electromagnetic fields and biological systems using both theoretical and experimental approaches, with particular reference to keywords as electroporation, smart drug delivery, molecular simulations of complex systems and implantable and wearable medical devices.